



Feature Article

An experimental and kinetic modeling study of *n*-propanol and *iso*-propanol combustion

Alessio Frassoldati^a, Alberto Cuoci^a, Tiziano Faravelli^a, Ulrich Niemann^b, Eliseo Ranzi^{a,*}, Reinhard Seiser^b, Kalyanasundaram Seshadri^b

^a Dipartimento di Chimica, Materiali e Ingegneria Chimica, Politecnico di Milano, 20133 Milano, Italy

^b Department of Mechanical and Aerospace Engineering, University of California at San Diego, 9500 Gilman Drive, Mail Code 0411, La Jolla, CA 92093-0411, USA

ARTICLE INFO

Article history:

Received 25 June 2009

Received in revised form 28 July 2009

Accepted 3 September 2009

Available online 6 October 2009

Keywords:

Alcohol fuels

Propanol combustion

Detailed kinetics

Counterflow flames

ABSTRACT

A kinetic model is developed to describe combustion of *n*-propanol and *iso*-propanol. It is validated by comparing predictions made using this kinetic model with new experimental data on structures of counterflow non-premixed flames and previously reported data over a wide range of configurations and conditions. The elementary pyrolysis reactions of methanol and ethanol are well-known and were used as a starting point for extension to propanol. A detailed description leading to evaluation of rate constants for initiation reactions, metathesis reactions, decomposition reactions, and four-center molecular dehydration reactions are given. Decomposition and oxidation of primary intermediate products are described using a previously developed semi-detailed kinetic model for hydrocarbon fuels. The kinetic mechanism is made up of more than 7000 reactions among 300 species. The structures of counterflow non-premixed flames were measured by removing gas samples from the flame and analyzing the samples using a gas chromatograph. The flame structures were measured under similar conditions for both fuels to elucidate the similarities and differences in combustion characteristics of the two isomers. The profiles measured include those of formaldehyde, acetaldehyde, propanal, and acetone. These species are considered to be pollutants. Validation of the kinetic model was first performed by comparing predictions with experimental data reported in the literature obtained in flow reactors and shock tubes. In these configurations, combustion is not influenced by molecular transport. The agreement between the kinetic model and experimental data was satisfactory. The predictions of the kinetic model were then compared with new and previously reported experimental data on structures of counterflow non-premixed flames of both isomers. The agreement between the kinetic model and experimental data was again satisfactory. Satisfactory agreement was also obtained when the predictions of the kinetic model were compared with experimental data obtained on low pressure burner stabilized premixed flames. The kinetic model was thus validated over a wide range of temperatures (from 900 K to 2000 K), and configurations. In general the structures and overall combustion characteristics of *n*-propanol flames and *iso*-propanol flames are similar. Acetone is formed under all conditions in *iso*-propanol flames, while propanal is formed in *n*-propanol flames.

© 2009 The Combustion Institute. Published by Elsevier Inc. All rights reserved.

1. Introduction

The need to limit the increase in greenhouse gas levels in the environment has motivated numerous studies on combustion of renewable fuels. Oxygen containing biofuels, in particular alcohols, show considerable promise, because they are considered to be neutral in regard to net greenhouse gas emissions to the environment. As a consequence, numerous experimental and modeling studies have been carried out to characterize combustion of methanol, ethanol, propanol (C₃H₇OH), and butanol [1–33]. Alcohols when used as additives to fossil fuels reduce the formation of polyaromatic hydrocarbon com-

pounds, particulates, and soot. Ethanol is widely used as biofuel additive to gasoline. Recent work suggests that use of alcohols as fuels has some deleterious effects on human health, due to high emission levels of toxic oxygenated by-products such as aldehydes [34]. Moreover, high concentrations of acetone ((CH₃)₂CO) were detected in the exhaust gas of a spark ignition engine upon addition of *iso*-propanol to a synthetic fuel [35]. The formation of oxygenated pollutants is a common feature of alcohol combustion that calls for detailed kinetic studies of the combustion chemistry of alcohol fuels [32]. Here, a kinetic modeling study of combustion of the propanol isomers, *n*-propanol and *iso*-propanol is carried out.

Only few kinetic studies of oxidation of *n*-propanol and *iso*-propanol are reported in the literature; they include experimental studies using batch [24–26] and flow reactors [10], shock-tubes

* Corresponding author.

E-mail address: eliseo.ranzi@polimi.it (E. Ranzi).

[33], co-flow diffusion flames [1], counterflow diffusion flames [29], droplet burning [30] and low-pressure premixed flat flames [31,32]. The combustion and pyrolysis of *n*-propanol has been also investigated in reflected shock waves with particular attention to the formation of soot and polycyclic aromatic hydrocarbons [23]. Fundamental investigations include studies on thermal decomposition of *iso*-propanol [27] and structures of flames over liquid pools [28]. The structure of non-premixed *iso*-propanol flames was measured previously employing the co-flow configuration [1] and the counterflow configuration [29]. The structure of diffusion flames depend on the stoichiometric mixture fraction and the strain rate [36–38]. The previous measurements of the structure of *iso*-propanol flames were made with the oxidizer stream made up of air enriched with oxygen [29]. The experimental conditions were characterized by high values of the stoichiometric mixture fraction and low values of the strain rates. Combustion in practical systems are characterized by low values of the stoichiometric mixture fraction and both low and high values of the strain rates [39]. To complement the previous studies new experimental data on the structure of counterflow diffusion flames of *n*-propanol and *iso*-propanol are presented in the next sections of the paper. The structure was measured with air as the oxidizer. The experimental conditions are characterized by low values of stoichiometric mixture fraction and moderately high values of strain rate. The new experimental data allow comparison of the flame structures of propanol isomers. The new experimental data together with previous experimental data are helpful in a further tuning and validation of the kinetic model of alcohol fuels.

2. Experimental measurements of flame structure

The structures of non-premixed flames of *n*-propanol and *iso*-propanol were measured employing the counterflow configuration. Fig. 1 shows a schematic illustration of the counterflow configuration. Steady, axisymmetric, laminar flow of two counter-flowing streams toward a stagnation plane is considered. In this configuration a fuel stream made up of prevaporized fuel (*n*-propanol or *iso*-propanol) and nitrogen is injected from the fuel duct, and an oxidizer stream of air is injected from the oxidizer duct. These jets flow into the mixing layer between the two ducts. The exit of the fuel duct is called the fuel boundary and the exit of the oxidizer duct the oxidizer boundary. The mass fraction of fuel, the temperature, and the component of the flow velocity normal to the stagnation plane at the fuel boundary are represented by $Y_{F,1}$, T_1 , and V_1 , respectively. The mass fraction of oxygen, the tempera-

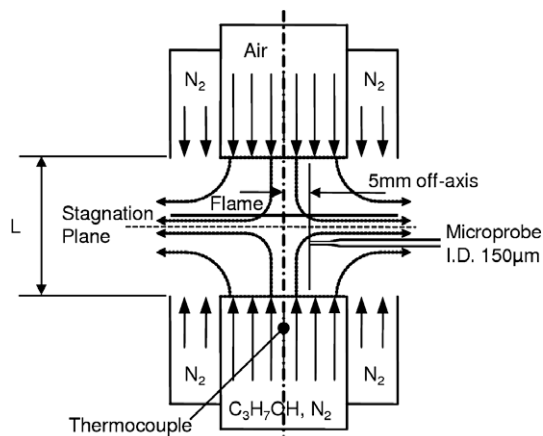


Fig. 1. Schematic illustration of the counterflow configuration. The figure shows the quartz microprobe used for measuring flame structure.

ture, and the component of the flow velocity normal to the stagnation plane at the oxidizer boundary are represented by $Y_{O_2,2}$, T_2 , and V_2 , respectively. The distance between the fuel boundary and the oxidizer boundary is represented by $L = 10$ mm.

The value of the strain rate, defined as the normal gradient of the normal component of the flow velocity, changes from the fuel boundary to the oxidizer boundary [40]. The characteristic strain rate on the oxidizer side of the stagnation plane a_2 is given by [40]

$$a_2 = \frac{2|V_2|}{L} \left(1 + \frac{|V_1|\sqrt{\rho_1}}{|V_2|\sqrt{\rho_2}} \right) \quad (1)$$

Here, ρ_1 and ρ_2 represent the density of the mixture at the fuel boundary and at the oxidizer boundary, respectively. The stoichiometric mixture fraction, Z_{st} is [36–38]

$$Z_{st} = (1 + \nu Y_{F,1}/Y_{O_2,2})^{-1} \quad (2)$$

where ν is the stoichiometric mass ratio of oxygen to fuel.

The profiles of concentration of stable species were measured for $Y_{F,1} = 0.3$, $T_1 = 353$ K, $Y_{O_2,2} = 0.233$, $T_2 = 298$ K, $a_2 = 97.5$ s⁻¹, $V_1 = 0.235$ m/s, $V_2 = 0.25$ m/s, and $L = 10$ mm. At these conditions the stoichiometric mixture fraction $Z_{st} = 0.2449$. Concentrations of stable species were measured by removing gas samples from the reaction zone using a heated quartz microprobe, and analyzing them in a gas chromatograph. The microprobe has a tip with an inner diameter of 150 µm. To minimize disturbances to the flow-field, the tip of the microprobe was placed at a location of 5 mm off the axis of symmetry as shown in Fig. 1. The location of the sampling probe in the flow-field was determined using a digital photo camera. The size of one pixel in the camera corresponds to a distance of approximately 20 µm in the flow-field. The mole fractions of various species in the sample were measured using an Agilent 3000microGC gas chromatograph. This instrument is equipped with a 10 m long molecular sieve 5A column, a 8 m long Poraplot U column, a 8 m long Poraplot Q column, and a 8 m long OV-1 column. The gas chromatograph has a built-in sample pump. To ensure equal sample sizes and thus comparable results across all measurements, a constant sample inlet pressure is required. Therefore species were sampled at a constant pressure of 600 mbar into a sample vessel. Nitrogen was then introduced until the vessel attained a total pressure of 1150 mbar. After a waiting period of 6 min, to allow sufficient mixing, the sample was drawn into the gas chromatograph. All lines from the sample probe to the gas chromatograph were heated to 373 K. The molecular sieve column uses argon as a carrier gas. It was used to separate hydrogen (H₂), oxygen (O₂), nitrogen (N₂), methane (CH₄), and carbon monoxide (CO). All other columns use helium as a carrier gas. The Poraplot U column was used for separating carbon dioxide (CO₂), ethylene (C₂H₄), ethane (C₂H₆), acetylene (C₂H₂), and formaldehyde (CH₂O). The Poraplot Q column was used for separating water (H₂O), propyne (C₃H₄), propylene (C₃H₆), propane (C₃H₈), acetaldehyde (C₂H₄O), butene (C₄H₈), butadiene (C₄H₆), acetone (C₃H₆O) and propanal (C₃H₆O). The OV-1 column was used for separating *n*-propanol and *iso*-propanol. The mole fractions of various species eluting from the columns were measured using thermal-conductivity detectors (TCD). The detectors were calibrated using samples of known composition. For those species that are liquids at room temperature and atmospheric pressure a sample vessel is used. First the sample vessel is evacuated. Next the liquid is injected with a syringe through a septum in the wall of the sample vessel. It is then diluted with nitrogen. The species fraction is determined from the pressure reading after evaporation. This procedure was used for *n*-propanol, *iso*-propanol, water, formaldehyde, propionaldehyde, and acetone. For those species that are gases at room temperature and atmospheric pressure, the calibration is performed with calibration gases of known composition. The peaks for all

species presented here show very good separation. Therefore, the expected accuracy for the maximum concentrations of all species except H₂O and CH₂O is expected to be better than ±10%. The expected accuracy for H₂O and CH₂O is better than ±20%. The accuracy for formaldehyde is based on the signal size compared to the baseline noise. The calibration for formaldehyde showed very little deviation and good repeatability.

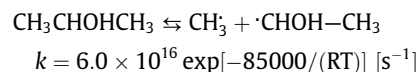
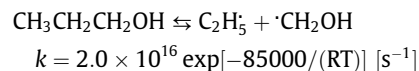
The experimental data obtained here are compared with calculated profiles. They are also compared with the experimental data of Sinha and Thompson [29]. These previous experimental data were obtained for $Y_{F,1} = 0.157$, $T_1 = 318$ K, $Y_{O_2,2} = 0.422$, $T_2 = 298$ K, $a_2 = 20.0$ s⁻¹, $V_1 = 0.10$ m/s, $V_2 = 0.10$ m/s, and $L = 20$ mm. At these conditions the stoichiometric mixture fraction $Z_{st} = 0.5283$.

3. Detailed kinetic mechanism of *n*-propanol and *iso*-propanol

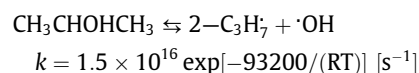
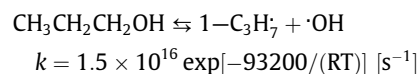
The pyrolysis and oxidation mechanisms of propanol isomers are very similar to those for hydrocarbon fuels. Therefore, the development of a complete set of the primary propagation reactions for these fuels requires the study and the definition of few new kinetic parameters for reactions involving bonds and H atoms near to the OH group. The elementary pyrolysis and oxidation reactions of methanol and ethanol are reasonably well-known and have been revised recently [9,10,13–16]. The kinetic mechanism for methanol and ethanol are a useful starting point for the extension to the kinetic schemes of *n*-propanol and *iso*-propanol. Initiation reactions are generally evaluated, by assuming a reference frequency factor with the activation energy equal to the bond energy, and microscopic reversibility based on the reverse radical recombination reaction is applied. Metathesis reactions require defining the reactivity of the H atoms in hydroxyl position and the H atoms in α position. Remaining H atoms are presumed to be unaffected by the presence of the OH group. Decomposition reactions of the corresponding alkoxy and parent radicals from alcohol fuels need further discussion. Isomerization reactions of these radicals are of limited importance and are neglected here. Finally, the class of the four-center molecular dehydration reactions requires careful attention. In this section, unimolecular reactions are discussed first followed by metatheses reactions, decomposition reactions of primary radicals from alcohol fuels, and four-center molecular dehydration reactions. The rate constant, k_i for reaction i is written as $k_i = A_i T^{n_i} \exp[-E_i/(RT)]$, where A_i is the frequency factor, E_i is the activation energy in cal/mol, T the temperature, n_i the temperature exponent, and R is the gas constant.

3.1. Unimolecular initiation reactions

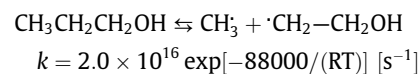
The activation energy of initiation reactions are evaluated from the strength of the C–C bond by defining the bond energy of primary and secondary C atoms (C_p and C_s) with OH substitutions. Thus,



The following kinetic parameters are prescribed for the reactions



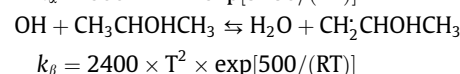
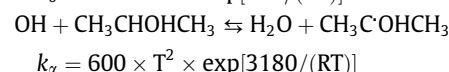
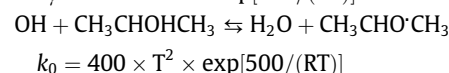
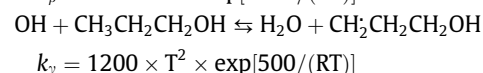
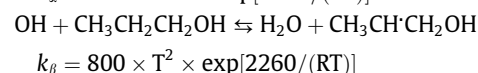
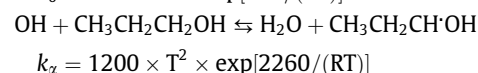
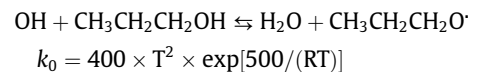
They are the same as that for the ethanol initiation reaction $\text{C}_2\text{H}_5\text{OH} \rightleftharpoons n\text{-C}_2\text{H}_5 + \cdot\text{OH}$. Note that these reference kinetic parameters are not affected by the nature of the C atom. More than 100 kcal/mol is required to release the H atom from the OH group, therefore reactions of this type cannot contribute to fuel decomposition. On the contrary, the reverse reactions could affect flame propagation. For this reason, all these reactions are included in the overall mechanism with the same kinetic parameter $k = 5.0 \times 10^{10}$ [l mol⁻¹ s⁻¹]. Kinetic data for the remaining initiation reactions, that involve the splitting of the C–C bond, are similar to those used for alkanes. Thus,



3.2. Metathesis reactions

The energy of the O–H bond in the OH group is greater than 100 kcal/mol and is similar to that of a C–H bond of primary H atoms in alkyl radicals. As assumed in the formation of methoxy and ethoxy radicals from methanol and ethanol, the kinetic parameters of this H-atom abstraction from the alcohol functional group are assumed to be equal to those for the abstraction of a primary H atom from a methyl group. Galano et al. [41] studied the gas phase reactions of alcohols with the OH radical employing a quantum mechanical approach. Moving away from the previous values recommended by Atkinson et al. [42,43], they concluded that the rate coefficient corresponding to the α channel (k_α) is larger than those of the other competing channels (k_β, k_γ, k_0), with the different channels reactivity order: $k_\alpha > k_\beta > k_\gamma > k_0$. The α branching ratio (Γ_α) for *n*-propanol goes from ~0.5 to 0.7, over the temperature range 290–500 K. These values are in line with the value 0.73 derived from the data recommended by Atkinson et al. [42,43]. The branching ratio $\Gamma_\beta = 0.12$ suggested by Dunlop and Tully [44] for *iso*-propanol agrees with the calculations developed by Galano et al. [41]. They confirm a value of ~0.10, thus supporting the higher reactivity of the H atoms of the α channel.

On the basis of these previous studies, we assume the following kinetic parameters for the H-abstraction reactions of OH radicals (units are: cal, l, mole, s, K):

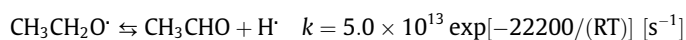
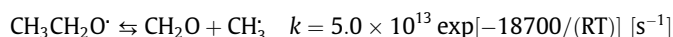


We preferred to maintain, also for these H sites, our systematic approach for metathesis reactions described elsewhere [45,46] and extensively used in the entire kinetic scheme [47]. Thus, kinetic parameters of H abstractions from CH₃–CH₂–CH₂–OH and from (CH₃)₂–CH–OH in α position are obtained by increasing by 50% the frequency factors of secondary and tertiary H atoms, respectively.

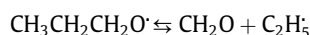
In this way, the α branching ratio for *n*-propanol is ~ 0.5 , and 0.6 for *iso*-propanol. Metathesis reactions of H, CH₃ and other abstracting radicals are treated according to the same approach.

3.3. Decomposition reactions of primary radicals from propanol

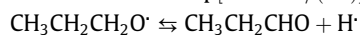
The expressions for the rate constants for C1–C4 alkyl and alkoxy radicals decomposition via β -scission have been revised recently [48]. Recommended rate parameters of the β -decomposition reactions are calculated using microscopic reversibility based on the reverse addition reactions of H or an alkyl radical to an olefin or carbonyl species. Recommended rate constants for C1–C4 alkoxy radical decompositions are based on an extensive study of available experimental data. Thus, ethoxy radical can decompose to form either formaldehyde and methyl radical, or acetaldehyde and a hydrogen atom, with the following suggested kinetic rates:



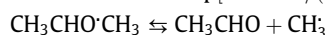
These rate expressions on one hand indicate a very high reactivity of alkoxy radicals, and on the other hand show a limited selectivity toward the dehydrogenation channel. In the temperature range 700–1000 K the first reaction channel that gives formaldehyde is favored by about a factor of ten. Even lower selectivity towards dehydrogenation paths are observed for C3 alkoxy radicals than those indicated above for C2 radical. Thus



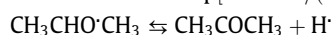
$$k = 5.0 \times 10^{13} \exp[-14700/(RT)] \text{ [s}^{-1}\text{]}$$



$$k = 5.0 \times 10^{13} \exp[-23100/(RT)] \text{ [s}^{-1}\text{]}$$



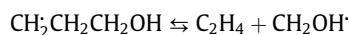
$$k = 5.0 \times 10^{13} \exp[-13000/(RT)] \text{ [s}^{-1}\text{]}$$



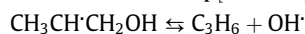
$$k = 5.0 \times 10^{13} \exp[-20700/(RT)] \text{ [s}^{-1}\text{]}$$

These considerations could lead to simplifications of the overall mechanism and the kinetic model. Alkoxy radicals do not significantly interact with the reacting system and could be considered instantaneously transformed into their final decomposition products. This limits the number of intermediate radical species involved in the overall kinetic scheme.

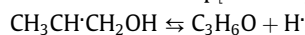
Kinetic data for decomposition reactions of alkyl radicals are the same as those used in the case of alkanes. The activation energy of reactions that involve the splitting of C–C or C–H bonds in α position of the OH group requires a careful analysis. Following previous work on ethanol decomposition, the following decomposition rates are assumed for *n*-propanol radicals:



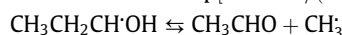
$$k = 3.0 \times 10^{13} \exp[-30000/(RT)] \text{ [s}^{-1}\text{]}$$



$$k = 3.0 \times 10^{13} \exp[-36000/(RT)] \text{ [s}^{-1}\text{]}$$



$$k = 6.0 \times 10^{13} \exp[-36000/(RT)] \text{ [s}^{-1}\text{]}$$

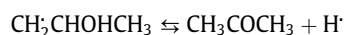


$$k = 3.0 \times 10^{13} \exp[-32500/(RT)] \text{ [s}^{-1}\text{]}$$



$$k = 6.0 \times 10^{13} \exp[-36000/(RT)] \text{ [s}^{-1}\text{]}$$

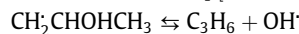
Similarly, the following decomposition reactions of *iso*-propanol radicals are postulated:



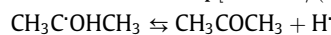
$$k = 6.0 \times 10^{13} \exp[-35000/(RT)] \text{ [s}^{-1}\text{]}$$



$$k = 3.0 \times 10^{13} \exp[-36000/(RT)] \text{ [s}^{-1}\text{]}$$

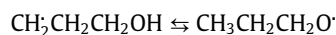


$$k = 3.0 \times 10^{13} \exp[-37000/(RT)] \text{ [s}^{-1}\text{]}$$



$$k = 6.0 \times 10^{13} \exp[-36000/(RT)] \text{ [s}^{-1}\text{]}$$

In these dehydrogenation reactions, the methyl-vinyl alcohol formed is presumed to be instantaneously transformed into acetone, via keto-enol tautomerism. The isomerization reactions of these radicals can be reasonably neglected, due to their very limited weight in respect of the corresponding decomposition reactions. Thus, the isomerization reaction of the primary radical of *n*-propanol to form the alkoxy radical, via a five membered ring intermediate:

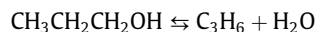


$$k = 1.0 \times 10^{11} \exp[-20600/(RT)] \text{ [s}^{-1}\text{]}$$

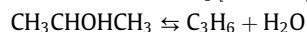
could become significant only at temperatures lower than 800 K. This is further enhanced for the reverse reaction of the alkoxy radical. The remaining isomerization reactions would require 4-membered ring intermediates and are therefore negligible.

3.4. Four-center molecular dehydration reactions

This class of reactions involves a four-center cyclic transition state with the formation of parent alkenes and H₂O, as shown in Fig. 2. Thus both propanol isomers form propylene with a four membered ring intermediate. Several kinetic parameters have been suggested for this class of reactions [12,13,19,20,27,49]. The following kinetic parameters are assumed for the dehydration reactions of the two propanol isomers:



$$k = 2.0 \times 10^{14} \exp[-67100/(RT)] \text{ [s}^{-1}\text{]}$$



$$k = 2.0 \times 10^{14} \exp[-67100/(RT)] \text{ [s}^{-1}\text{]}$$

These values for the rate constants are consistent with the recent kinetic analysis of *n*-butanol dehydration reactions [21]. This reaction is endothermic by 8.25 kcal/mol with an associated activation enthalpy of ~ 67.5 kcal/mol. Fig. 3 is a schematic illustration of *n*-propanol and *iso*-propanol decomposition. The detailed sub-mechanism of *n*-propanol and *iso*-propanol is reported in Table 1. Further decomposition and/or oxidation reactions of primary intermediate products are described in a semi-detailed oxidation mechanism for hydrocarbon fuels up to C16 developed in previous studies [47,50]. The overall kinetic scheme is based on hierarchical

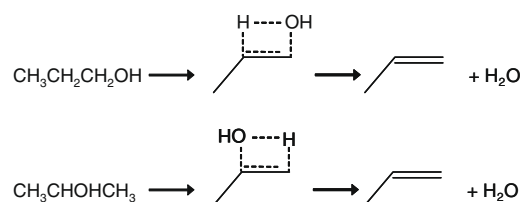


Fig. 2. Dehydration reactions of *n*-propanol and *iso*-propanol to form propylene.

modularity and is made up of more than 7000 reactions among 300 species. Thermochemical data for most species was obtained from the CHEMKIN thermodynamic database [51,52]. For those species for which thermochemical data is not available in the literature, the group additive method was used to estimate these properties [53]. The complete mechanism, with thermochemical and transport properties, is available online in CHEMKIN format [54].

4. Numerical methods and simulations

The kinetic model described in the previous section was validated by comparing the results of numerical simulations with new and previous experimental data on counterflow non-premixed flames, and available experimental data obtained employing shock tube and flow reactor.

The DSMOKE code was used to numerically solve the system of equations that describe various aspects of combustion in shock tube and ideal flow reactor [55]. To predict aspects of combustion that include molecular transport and chemical reactions a 1-D laminar flame model was employed. A detailed description of this code is given elsewhere [56]. This code includes multicomponent diffusion and thermal diffusion. Discretization of the differential equations is carried out using conventional finite differencing techniques for non-uniform mesh spacing. The numerical problem corresponds to a large system of differential-algebraic equations (DAE). The specifically conceived methods and solver routines of BzzMathLibrary [57,58] are used to handle the complexity of this numerical problem. More than 300 grid points are used to ensure

grid-insensitive results. This 1-D laminar flame code is used here to predict the structure of counterflow non-premixed flames and premixed flames. In premixed burner-stabilized flames experiments there are often significant heat losses to the burner which are difficult to estimate. Therefore, in the numerical simulations the measured temperature profile is used as an input parameter. As a consequence, for premixed flames, the energy conservation equation is not included in the system of equations that are solved. The boundary conditions employed in flame calculations are identical to those in the experiments.

5. Model predictions and comparisons with experimental data

Norton and Dryer [10] studied the oxidation of propanol isomers in a flow reactor at atmospheric pressure, temperatures of 1000–1100 K and residence time of ~ 0.1 s. They investigated propanol oxidation under fuel lean conditions with high N_2 dilution. Recently ignition delay times have been measured for *n*-propanol and *iso*-propanol in shock tubes [33]. New experimental data on the structure of counterflow non-premixed *n*-propanol and *iso*-propanol flames have been obtained and are discussed later. Similar non-premixed flames of pure *iso*-propanol and different mixtures with propane were investigated by Sinha and Thomson [29].

Kasper et al. [32] studied the combustion of the two propanol isomers in low-pressure, premixed flat flames using two independent MBMS techniques. For each alcohol, a set of three flames at ~ 2000 K with different stoichiometries was measured, providing an extensive data base. Profiles of stable and intermediate species,

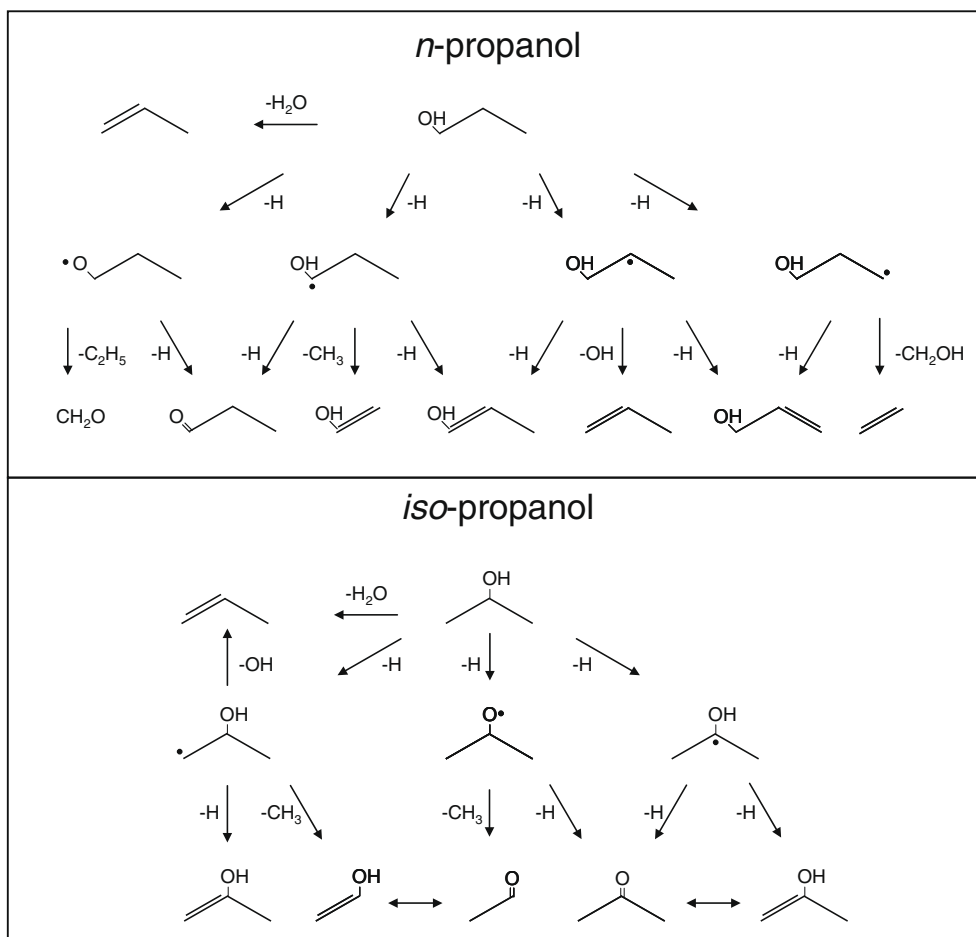


Fig. 3. Reaction mechanism of *n*-propanol and *iso*-propanol decomposition.

Table 1
Sub-mechanisms of *n*- and *iso*-propanol decomposition.

	Reaction ^a	<i>A</i>	<i>n</i>	<i>E_a</i>
<i>n</i> -Propanol				
1	$n\text{C}_3\text{H}_7\text{OH} \rightleftharpoons \text{CH}_3 + \text{C}_2\text{H}_4\text{OH}$	2.0×10^{16}	0	88,000
2	$n\text{C}_3\text{H}_7\text{OH} \rightleftharpoons \text{C}_2\text{H}_5 + \text{CH}_2\text{OH}$	2.0×10^{16}	0	85,000
3	$n\text{C}_3\text{H}_7\text{OH} \rightleftharpoons \text{OH} + n\text{C}_3\text{H}_7$	1.5×10^{16}	0	92,300
4	$n\text{C}_3\text{H}_7\text{OH} \rightleftharpoons \text{CH}_2\text{CH}_2\text{CH}_2\text{OH} + \text{H}$	3.6×10^{19}	-1	102,800
5	$n\text{C}_3\text{H}_7\text{OH} \rightleftharpoons \text{CH}_3\text{CHCH}_2\text{OH} + \text{H}$	1.8×10^{19}	-1	99,600
6	$n\text{C}_3\text{H}_7\text{OH} \rightleftharpoons \text{CH}_3\text{CH}_2\text{CHOH} + \text{H}$	7.7×10^{18}	-1	97,400
7	$\text{R} + n\text{C}_3\text{H}_7\text{OH} \rightarrow \text{RH} + \text{CH}_2\text{CH}_2\text{CH}_2\text{OH}$	$3H_{\text{Prim}}$		
8	$\text{R} + n\text{C}_3\text{H}_7\text{OH} \rightarrow \text{RH} + \text{CH}_3\text{CHCH}_2\text{OH}$	$2H_{\text{Sec}}$		
9	$\text{R} + n\text{C}_3\text{H}_7\text{OH} \rightarrow \text{RH} + \text{CH}_3\text{CH}_2\text{CHOH}$	$2H_{\text{Sec}}^{\text{OH}}$		
10	$\text{R} + n\text{C}_3\text{H}_7\text{OH} \rightarrow \text{RH} + \text{CH}_3\text{CH}_2\text{CH}_2\text{O}$	$1H_{\text{Prim}}$		
11	$\text{CH}_3\text{CH}_2\text{CH}_2\text{O} \rightleftharpoons \text{C}_2\text{H}_4 + \text{C}_2\text{H}_5$	5.0×10^{13}	0	14,700
12	$\text{CH}_2\text{CH}_2\text{CH}_2\text{OH} \rightleftharpoons \text{C}_2\text{H}_4 + \text{CH}_2\text{OH}$	3.0×10^{13}	0	30,000
13	$\text{CH}_2\text{CH}_2\text{CH}_2\text{OH} \rightleftharpoons \text{H} + \text{C}_3\text{H}_5\text{OH}$	3.0×10^{13}	0	36,000
14	$\text{CH}_3\text{CHCH}_2\text{OH} \rightleftharpoons \text{C}_3\text{H}_6 + \text{OH}$	3.0×10^{13}	0	36,000
15	$\text{CH}_3\text{CHCH}_2\text{OH} \rightleftharpoons \text{H} + \text{C}_2\text{H}_5\text{CHO}$	6.0×10^{13}	0	36,000
16	$\text{CH}_3\text{CH}_2\text{CHOH} \rightleftharpoons \text{CH}_3\text{CHO} + \text{CH}_3$	3.0×10^{13}	0	32,500
17	$\text{CH}_3\text{CH}_2\text{CHOH} \rightleftharpoons \text{H} + 0.5\text{C}_2\text{H}_5\text{CHO} + 0.5\text{C}_3\text{H}_5\text{OH}$	6.0×10^{13}	0	36,000
18	$\text{O}_2 + \text{CH}_2\text{CH}_2\text{CH}_2\text{OH} \rightleftharpoons \text{HO}_2 + \text{C}_2\text{H}_5\text{CHO}$	1.5×10^9	0	5000
19	$\text{O}_2 + \text{CH}_3\text{CHCH}_2\text{OH} \rightleftharpoons \text{HO}_2 + 0.5\text{C}_2\text{H}_5\text{CHO} + 0.5\text{C}_3\text{H}_5\text{OH}$	1.5×10^9	0	5000
20	$\text{O}_2 + \text{CH}_3\text{CH}_2\text{CHOH} \rightleftharpoons \text{HO}_2 + \text{C}_3\text{H}_5\text{OH}$	1.5×10^9	0	5000
21	$n\text{C}_3\text{H}_7\text{OH} \rightleftharpoons \text{C}_3\text{H}_6 + \text{H}_2\text{O}$	2.0×10^{14}	0	67,100
<i>iso</i> -Propanol				
1	$i\text{C}_3\text{H}_7\text{OH} \rightleftharpoons \text{CH}_3 + \text{CH}_3\text{CHOH}$	6.0×10^{16}	0	85,000
2	$i\text{C}_3\text{H}_7\text{OH} \rightleftharpoons \text{OH} + i\text{C}_3\text{H}_7$	1.5×10^{16}	0	93,200
3	$i\text{C}_3\text{H}_7\text{OH} \rightleftharpoons \text{CH}_3\text{COHCH}_3 + \text{H}$	7.0×10^{18}	-1	97,800
4	$i\text{C}_3\text{H}_7\text{OH} \rightleftharpoons \text{CH}_3\text{CHOHCH}_2 + \text{H}$	3.3×10^{19}	-1	103,200
5	$\text{R} + i\text{C}_3\text{H}_7\text{OH} \rightarrow \text{RH} + \text{CH}_3\text{CHOCH}_3$	$1H_{\text{Prim}}$		
6	$\text{R} + i\text{C}_3\text{H}_7\text{OH} \rightarrow \text{RH} + \text{CH}_3\text{CHOHCH}_2$	$6H_{\text{Prim}}$		
7	$\text{R} + i\text{C}_3\text{H}_7\text{OH} \rightarrow \text{RH} + \text{CH}_3\text{COHCH}_3$	$2H_{\text{Tert}}^{\text{OH}}$		
8	$\text{CH}_3\text{CHOCH}_3 \rightleftharpoons \text{CH}_3 + \text{CH}_3\text{CHO}$	5.0×10^{13}	0	13,000
9	$\text{CH}_3\text{CHOCH}_3 \rightleftharpoons \text{CH}_3\text{COCH}_3 + \text{H}$	5.0×10^{13}	0	20,700
10	$\text{CH}_3\text{CHOHCH}_3 \rightleftharpoons \text{CH}_3\text{COCH}_3 + \text{H}$	6.0×10^{13}	0	36,000
11	$\text{CH}_3\text{CHOHCH}_2 \rightleftharpoons \text{CH}_3 + \text{CH}_3\text{CHO}$	3.0×10^{13}	0	36,000
12	$\text{CH}_3\text{CHOHCH}_2 \rightleftharpoons \text{CH}_3\text{COCH}_3 + \text{H}$	6.0×10^{13}	0	35,000
13	$\text{CH}_3\text{CHOHCH}_2 \rightleftharpoons \text{C}_3\text{H}_6 + \text{OH}$	3.0×10^{13}	0	37,000
14	$\text{O}_2 + \text{CH}_3\text{COHCH}_3 \rightleftharpoons \text{HO}_2 + \text{CH}_3\text{COCH}_3$	1.5×10^9	0	5000
15	$\text{O}_2 + \text{CH}_3\text{CHOHCH}_2 \rightleftharpoons \text{HO}_2 + \text{CH}_3\text{COCH}_3$	1.5×10^9	0	5000
16	$i\text{C}_3\text{H}_7\text{OH} \rightleftharpoons \text{C}_3\text{H}_6 + \text{H}_2\text{O}$	2.0×10^{14}	0	67,100

^a $k = A \cdot T^n \cdot \exp(-E_a/RT)$. Units are: mole, l, s, K and cal.

including several radicals, were measured as a function of height above the burner. Finally, Li et al. [31] investigated lean and rich premixed flames of *n*-propanol and *iso*-propanol at low pressure, aiming at a better understanding of the combustion chemistry of C3 alcohols. They used the synchrotron photoionization and molecular-beam mass spectrometry (PI-MBMS) techniques to measure radical intermediates and stable species in the flame [31]. Validation of the kinetic mechanism was carried out over a wide range by comparing predictions with experimental data obtained: (1) in flow reactors [10], (2) ignition delay times measured in shock tube [33], (3) new and previous [29] measurements of structures of counterflow non-premixed flames, and (4) low-pressure premixed flames [31,32]. While the complete set of predicted results and relevant comparisons with the experimental measurements is reported in the [Supplemental material](#), the key and crucial features are described in the following sections.

5.1. Flow reactor at atmospheric pressure

Figs. 4 and 5 compare predictions of the kinetic model with experimental data obtained in flow reactor [10]. Fig. 4 shows comparison for *n*-propanol and Fig. 5 for *iso*-propanol. The agreement between model predictions and experimental measurements are satisfactory. Note that, following usual practice employed for comparison with flow reactor data [16], predicted profiles are shifted by ~20–30 ms in order to account for non-ideal reactant mixing.

Moreover, to better match the fuel conversion, predicted profiles are obtained with the input temperature profile increased by ~5–10 K above the measured profile for both the fuels. Experimental data clearly confirm the higher reactivity of *n*-propanol with respect to *iso*-propanol. Propylene (C_3H_6) yields from *iso*-propanol are higher than 35% while less than one half is obtained from *n*-propanol. The larger propylene formation from *iso*-propanol is mainly due to the molecular dehydration reaction of the fuel. As shown in Fig. 3, H-abstraction reactions form three different intermediate radicals $\text{C}_3\text{H}_7\text{O}$ whose major decomposition product is acetone. *n*-Propanol is the most reactive of the two isomers, due to the larger importance of radical pathways with the significant formation of propanal ($\text{C}_2\text{H}_5\text{CHO}$). Acetone yield from *iso*-propanol peaks to ~20%, while the maximum yield of propanal from *n*-propanol is ~10%. Radical decomposition paths prevail on the *n*-propanol decomposition. As usual, H-abstraction reactions of OH and H radicals are the dominant ones (~65% and ~25%, respectively), with a minor role of methyl (~7%) and oxygen radicals. On the contrary, molecular dehydration of *iso*-propanol is the main source of propylene and it accounts for more than 50% of the overall conversion in these conditions. It seems relevant to underline that ethylene (C_2H_4) is only a secondary product of *iso*-propanol, its scarce formation moves through the H addition to propylene, the formation of 1-propyl radical and the successive de-methylation reaction. On the contrary the formation of ethane (C_2H_6), due to the recombination reactions of methyl radicals, is over-predicted.

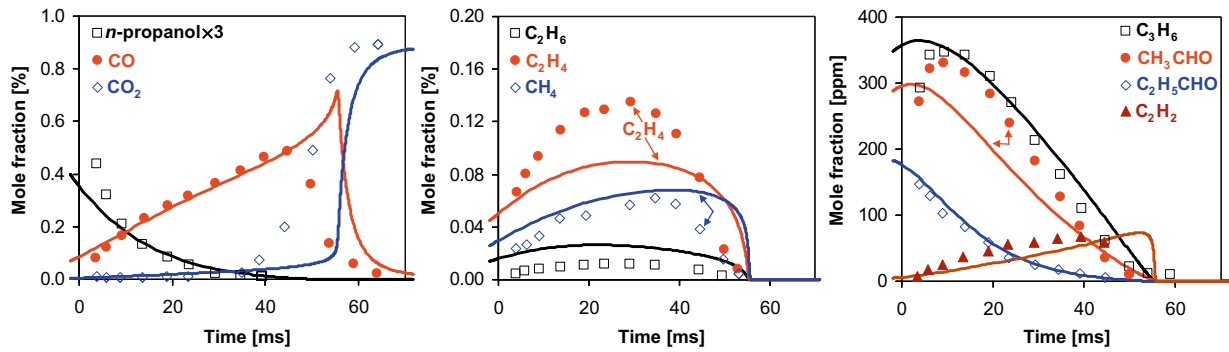


Fig. 4. Comparison of predictions of the kinetic model with experimental data obtained in flow reactor for *n*-propanol. The symbols represent experimental data [10] and the curves are predictions of the kinetic model.

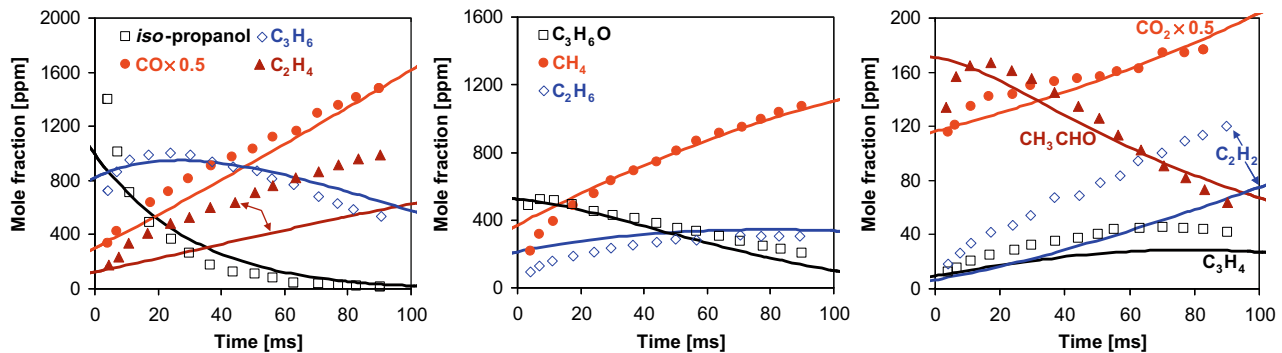


Fig. 5. Comparison of predictions of the kinetic model with experimental data obtained in flow reactor for *iso*-propanol. The symbols represent experimental data [10] and the curves are predictions of the kinetic model.

Methane is well predicted and this seems to indicate a reasonable concentration of methyl radicals. The large formation of ethylene, and model under-prediction, could also induce perplexity on the accuracy of ethane–ethylene separation.

Other minor products, such as propadiene (C_3H_4) and allene and C_4 species are also well predicted. The experimental data of thermal decomposition of *iso*-propanol in a batch reactor at 0.058 bar and 766 K (Trenwith [26]) allow to better validate the radical paths. In fact, molecular dehydration reaction is not significant at these conditions. The 30% *iso*-propanol decomposition observed and properly predicted by the model after ~ 400 s is only due to the radical reaction mechanism. Pyrolysis of both *n*-propanol and *iso*-propanol at temperatures of 800–900 K in a closed batch reactor was also investigated by Barnard and Hughes [24] and Barnard [25]. Model prediction underestimates propanol conversion by a factor of ~ 2 for both the fuels. According to the experimental measurements, model prediction confirms that pyrolysis of *iso*-propanol is faster than the corresponding one of *n*-propanol, in these conditions. The formation of tar components and the large deficit in the C/H/O balances observed in experimental data does not allow detailed comparisons of model predictions with experimental data.

5.2. Ignition delay times in shock tube

Recently, ignition delay times of reactive mixtures of either *n*-propanol or *iso*-propanol with oxygen and argon have been measured behind reflected shock waves at high temperatures (1350–2000 K) and atmospheric pressure [33]. Fuel-lean, stoichiometric and fuel-rich mixtures were considered. Pressure measurements and CH^+ emissions were used to determine ignition delay times. The influence of temperature and stoichiometry on ignition delay

times has been characterized and also compared to the predictions of a detailed kinetic mechanism currently under development [33]. This study and experimental data [33] shows the similar behavior of the two fuels confirming the greater reactivity of *n*-propanol relative to corresponding mixtures of *iso*-propanol only at low temperatures. The kinetic model developed here was also used to predict the ignition delay times. Fig. 6 compares the predictions of ignition delay times [μs] as a function of $1000/T$, with experimental data. Here T is the initial temperature of the reactive mixture. The numerical simulations were performed for values of equivalence ratio, Φ equal to 0.5, 1.0, and 2.0. For $\Phi = 1.0$, and $\Phi = 2.0$, the fuel mass fraction in the reactive mixture was 0.005, and for $\Phi = 0.5$ the fuel mass fraction was 0.0025. The predictions of the kinetic model agrees well with experimental data at low temperatures. Larger deviations between predictions and data are mainly observed at temperatures higher than 1700 K. The relevant curvature at high temperature is not reproduced by the model. The apparent activation energies predicted are in the order of 45–50 kcal/mol, while those calculated using the measured data are lower than 35 kcal/mol. This clearly points to further experimental and kinetic modeling analysis.

5.3. Counterflow non-premixed flame of *n*-propanol and *iso*-propanol

Experimental measurements on counterflow non-premixed flames discussed in Section 2 are compared with model predictions in Figs. 7 and 8. Fig. 7 shows the structure of a non-premixed *iso*-propanol flame while Fig. 8 shows the structure of a non-premixed *n*-propanol flame. These figures show the mole fraction of various species as a function of distance from the fuel boundary. The symbols in these figures represent experimental data and the lines are model prediction. The profiles in these figures were obtained at a

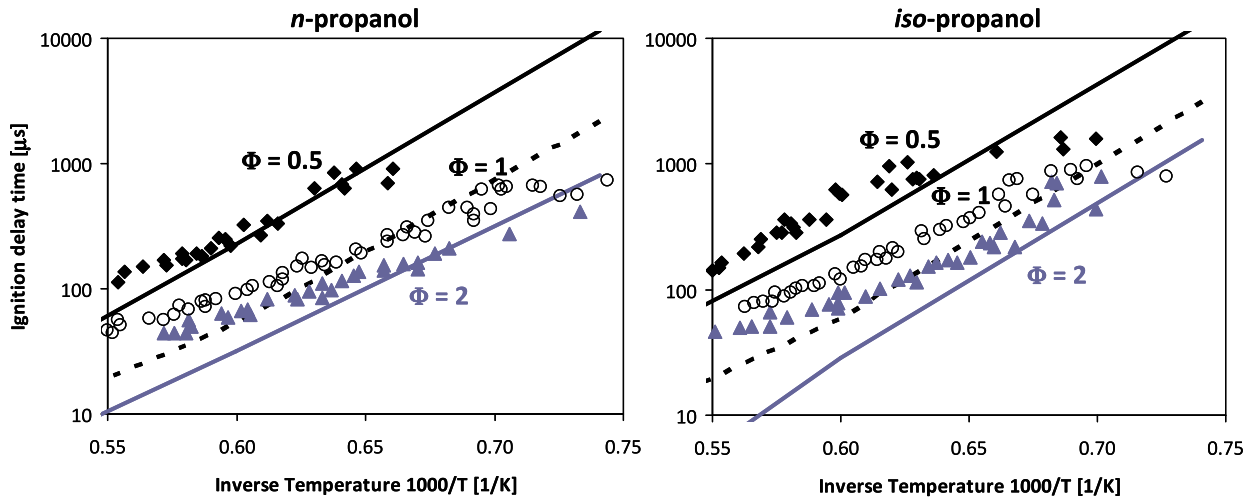


Fig. 6. Comparison of predictions of ignition delay times [μs], as a function of the reciprocal of temperature, obtained using the kinetic model with experimental data obtained in shock tube [33] for *n*-propanol and *iso*-propanol. The symbols represent experimental data [33] and the lines are predictions of the kinetic model.

strain rate $a_2 = 97.5 \text{ s}^{-1}$, and the stoichiometric mixture fraction $Z_{st} = 0.2449$. There are a number of similarities between the flame structure of these isomers. The measured profile of ethylene shows that the concentration of this compound is higher in the *n*-propanol

flame in comparison to its concentration in the *iso*-propanol flame. This large difference in ethylene peaks is properly predicted. As already mentioned, ethylene is only a secondary product in *iso*-propanol decomposition. This fact is well evident in Fig. 9, which

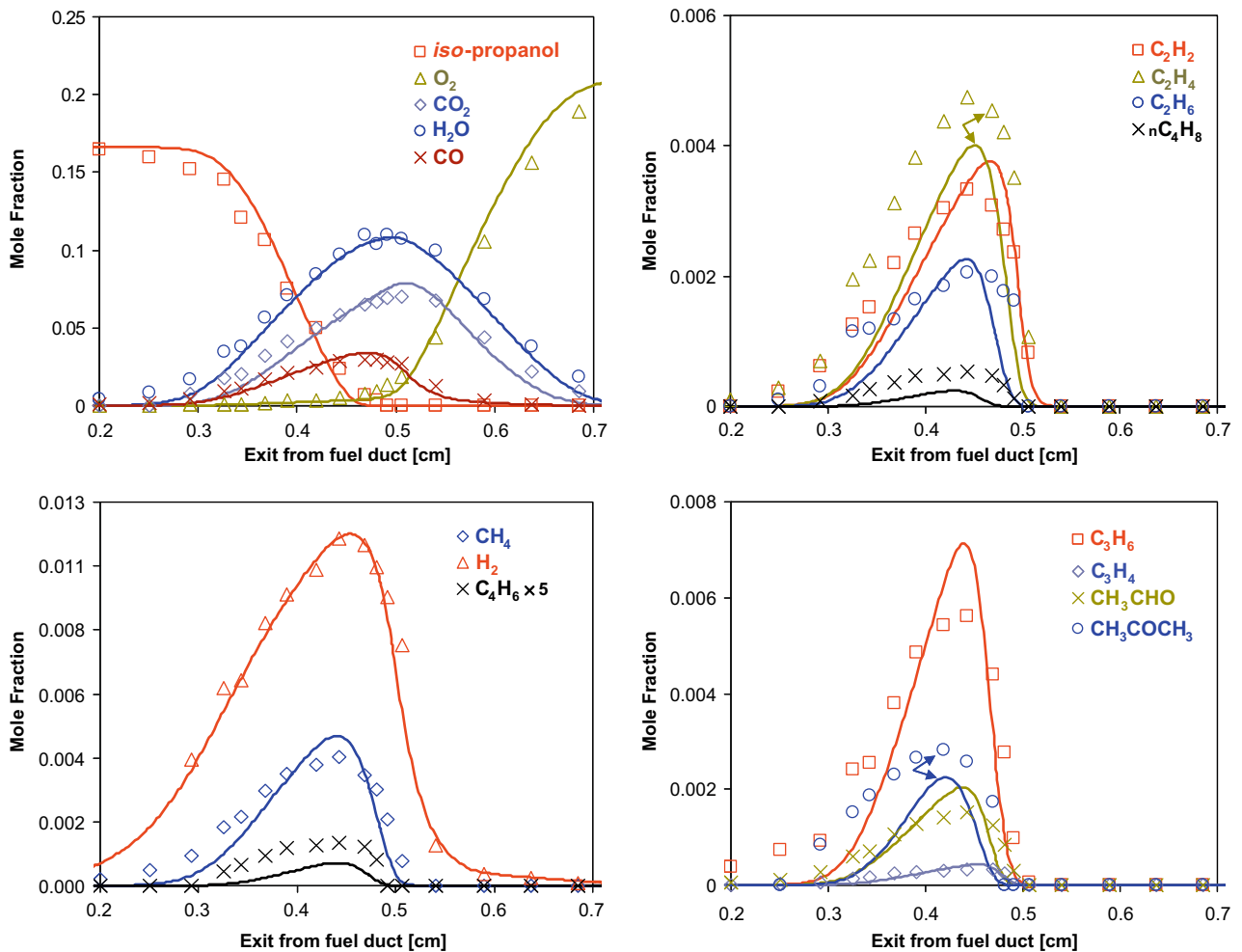


Fig. 7. Profiles of mole fraction of various species as a function of distance from the fuel boundary for non-premixed *iso*-propanol flames at a value of the strain rate $a_2 = 97.5 \text{ s}^{-1}$, and the stoichiometric mixture fraction $Z_{st} = 0.2449$. The symbols represent experimental data and the lines are model predictions.

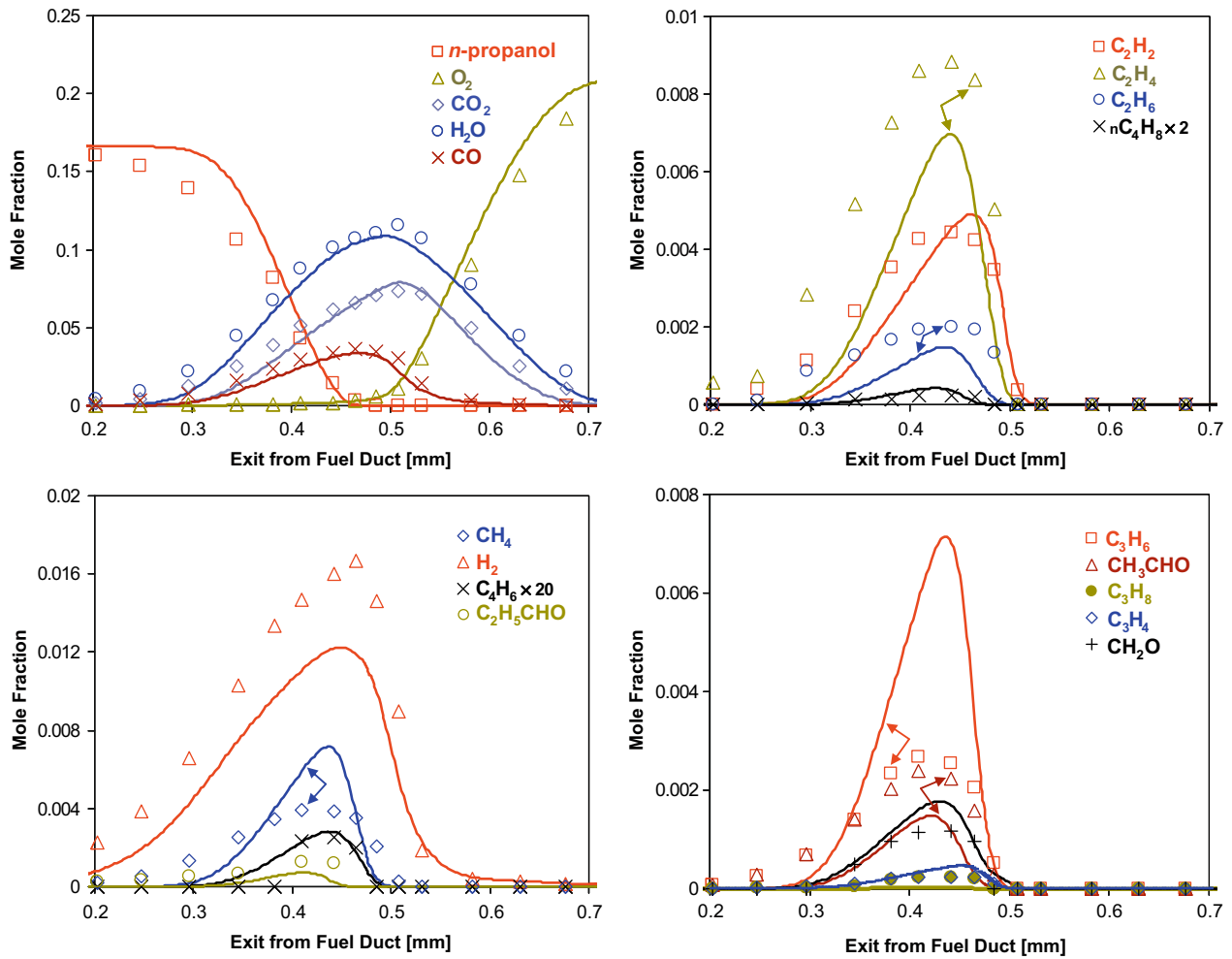
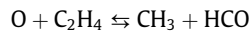


Fig. 8. Profiles of mole fraction of various species as a function of distance from the fuel boundary for non-premixed *n*-propanol flames at a value of the strain rate $a_2 = 97.5 \text{ s}^{-1}$, and the stoichiometric mixture fraction $Z_{st} = 0.2449$. The symbols represent experimental data and the lines are model predictions.

shows the reaction flux analysis of the two flames. Ethylene formation from *iso*-propanol is only due to the dehydrogenation of ethyl radicals (formed via recombination of methyl radicals leading to ethane and successive H abstractions) and to the de-methylation of *n*-propyl radical (formed via H addition reaction on propylene). On the contrary, primary ethylene formation from *n*-propanol is also sustained by the β -decomposition reaction of the $\cdot\text{CH}_2\text{CH}_2\text{CH}_2\text{OH}$ radical (see Fig. 3). In *iso*-propanol and *n*-propanol flames, ethylene consumption is mainly due to the H-abstraction

reactions to form vinyl radical in the fuel region and to the addition reaction of O radical in the flame front:



The kinetic model satisfactorily predicts the profile of acetone in *n*-propanol flame (Fig. 8) and propanal in *iso*-propanol flame (Fig. 7). Fig. 10 shows the structure of a non-premixed *iso*-propanol flame measured by Sinha and Thompson [29] at a strain rate $a_2 = 20 \text{ s}^{-1}$, and the stoichiometric mixture fraction $Z_{st} = 0.5283$.

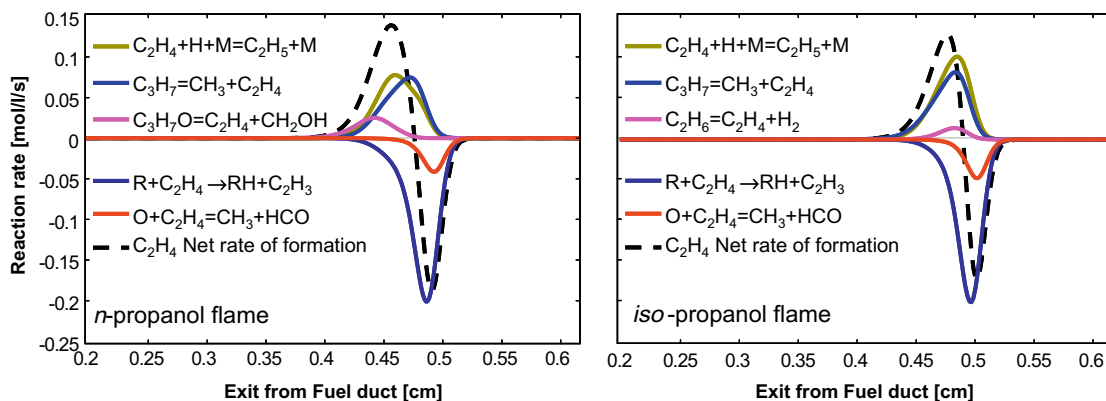


Fig. 9. Reaction flux analysis of ethylene formation in propanol flames of Figs. 7 and 8.

The symbols represent experimental data [29] and the lines are model predictions. Comparison of Figs. 7 and 10 shows the influence of strain rate and stoichiometric mixture fraction on flame structure. The agreement between the predicted and measured profiles of oxygenated and C2 species is satisfactory. Fig. 7 shows that the predicted profile of propylene agrees with experimental data, while the predicted profile of propylene in Fig. 10 exceeded the experimental data approximately by a factor of 2. These data are useful both in order to confirm the experimental measurements and to verify the possible systematic deviations between model predictions and experiments.

5.4. Low-pressure premixed flames of *n*-propanol and *iso*-propanol

Kasper et al. [32] carried out an experimental study of combustion of *n*-propanol and *iso*-propanol in low-pressure, premixed flat flames using two complementary molecular-beam mass spectrometry (MBMS) techniques: electron ionization (EI) and photon ionization (PI). The equivalence ratio of the reactive mixture, Φ , considered was 1, 1.5 and 1.9.

Profiles of various species were calculated employing the kinetic model described here. Predicted profiles were shifted by 1.5–2 mm to better match flame structure and maxima of intermediate species. These values are within the experimental uncertainties for the measured temperature profiles. For all flames tested

good agreement was obtained between model predictions and experimental data for major species. As observed by Kasper et al. [32], the structures of *n*-propanol flame and *iso*-propanol flame are similar. Differences were mainly observed in the primary oxygenated products as well as in ethylene that is a secondary product in the *iso*-propanol flames. Further detail of model comparisons with the experimental measurements of both sets of *n*-propanol and *iso*-propanol flames at $\Phi = 1.0, 1.5$ and 1.9 are available in the Supplemental material.

Figs. 11 and 12 show comparison of predicted profiles of major intermediate species with experimental data for $\Phi = 1.0$, and $\Phi = 1.9$. Fig. 11 shows comparison for *iso*-propanol flame and Fig. 12 for *n*-propanol flame. Experimental measurements shown in these figures include those obtained by Kasper et al. [32] using electron EI and PI techniques. Figs. 13 and 14 show similar comparison of methyl (CH_3) and propargyl (C_3H_3) radicals, for both the fuels. Benzene production in the rich flames is well predicted by the model and is similar for both the fuels, although it is possible to observe a larger formation from *iso*-propanol flame.

Fig. 15 reports the sensitivity analysis to benzene formation. Benzene is mainly formed from propargyl radicals in both the cases, thus all the reactions favoring propylene, allene as well as allyl and propargyl radicals formation show a positive sensitivity coefficient. On the contrary, all the propagation reactions favor benzene depletion. It is also noteworthy that benzene peak is high-

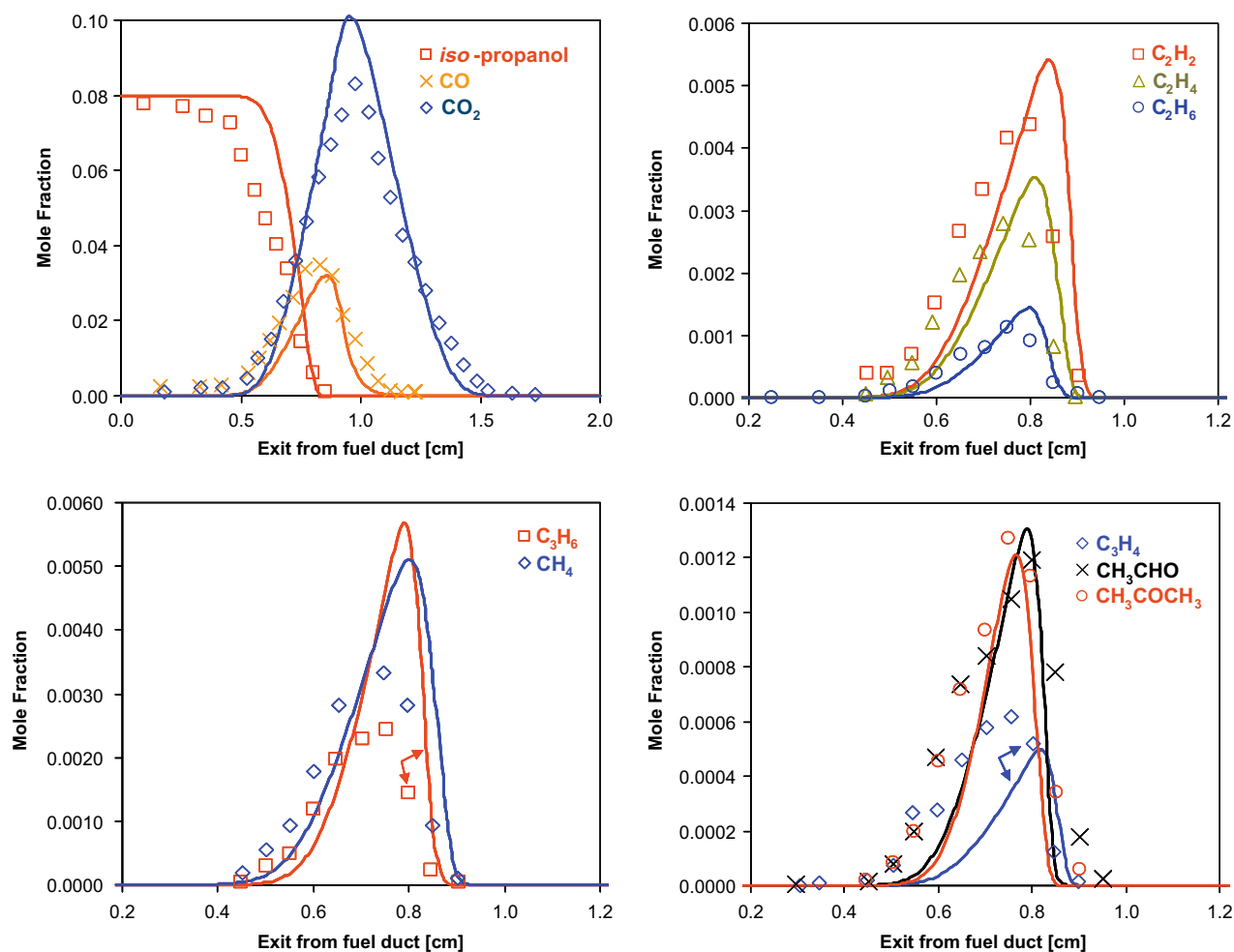


Fig. 10. Profiles of mole fraction of various species as a function of distance from the fuel boundary for non-premixed *iso*-propanol flames at a value of the strain rate $a_2 = 20 \text{ s}^{-1}$, and the stoichiometric mixture fraction $Z_{st} = 0.5283$. The symbols represent experimental data obtained by Sinha and Thompson [29] and the lines are model predictions.

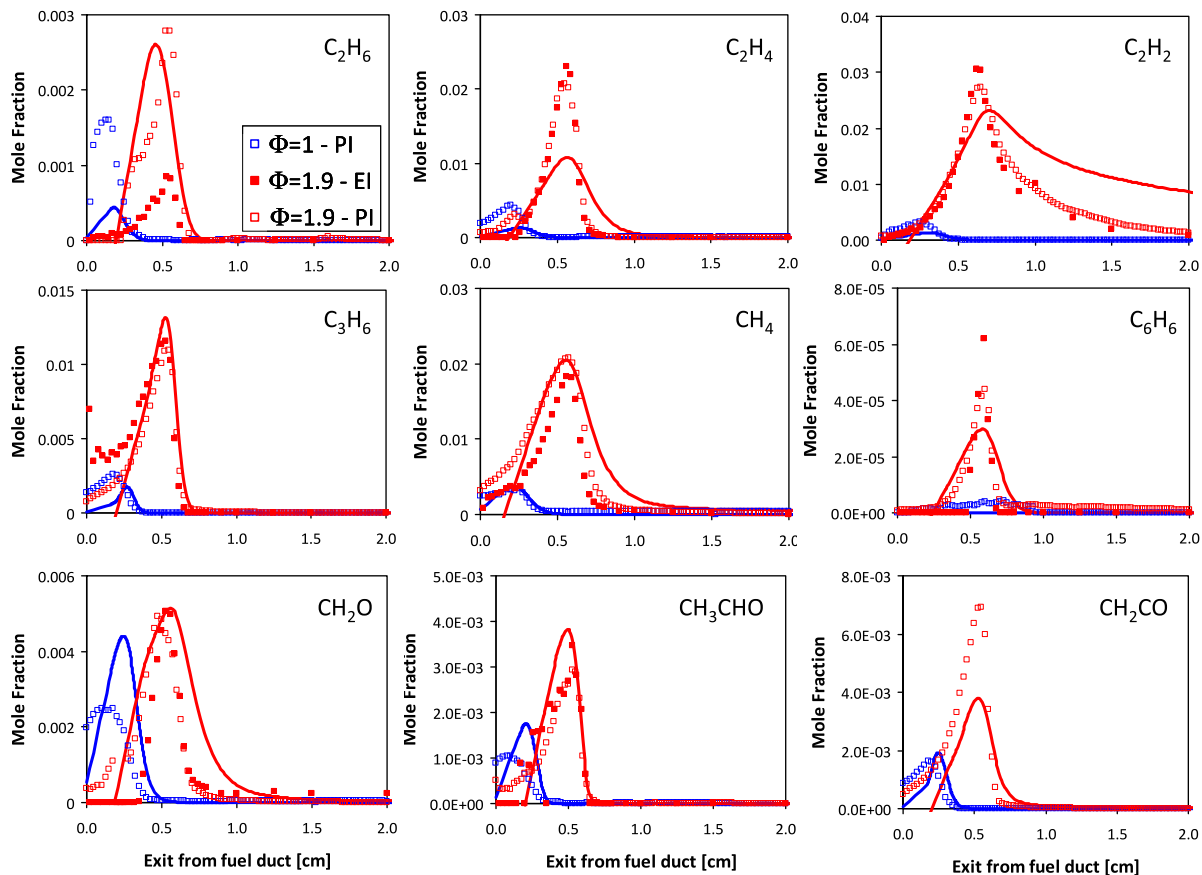


Fig. 11. Profiles of mole fraction of various intermediate species as a function of distance from the fuel duct. The fuel tested is *iso*-propanol. The equivalence ratio is $\Phi = 1$, and $\Phi = 1.9$. The symbols represent experimental data measured by Kasper et al. [32] using electron ionization (EI) and photon ionization (PI) molecular-beam mass spectrometry. The curves are model predictions.

er and it occurs later in the *iso*-propanol flame, due to the lower reactivity and the larger presence of methyl radicals.

Studies on premixed laminar flames of *iso*-propanol and *n*-propanol at low pressure were recently carried out by Li et al. [31]. The complete simulation results are reported in the [Supplemental material](#). Table 2 shows a comparison between measured and predicted peak positions and corresponding maximum mole fractions in both the rich flames ($\Phi = 1.8$). Predicted profiles are shifted of about 4–5 mm to match measured flame structure and maxima of intermediate species. It is noteworthy to observe again that there exists strong similarity between the two flames. Moreover is of interest to observe the similarity between these flames and the corresponding ones studied by Kasper et al. [32].

Table 2 shows that although the predicted peak values and positions of several species, including acetone and propanal, agree well with the experimental measurements, large discrepancies are also evident for some species and they require some comments. The availability of two other sets of independent experimental measurements, resulting from the work of Kasper et al. [32] and Li et al. [31], allows to better evaluating the meaning and importance of these deviations. The following summarizes some observations of the comparisons shown in Table 2:

Acetylene: The observed over-prediction of acetylene for the *iso*-propanol flame is not consistent with the slight under-prediction reported in Fig. 12.

Vinyl radical: This species is largely over-predicted for both fuels. These experimental measurements do not agree with the corresponding measurements, both with EI and PI techniques of Kasper [59].

Formyl radical: This species is largely over-predicted for both fuels. These experimental measurements do not agree with the corresponding measurements with PI technique of Kasper [59]. Ethyl radical, with atomic mass 29, is $\sim 1 \times 10^{-5}$ is completely covered by formyl radical.

Allyl radical: This species is again 10 times over-predicted for both fuels. The measurements of Kasper [59] employing the PI technique indicate that for the *iso*-propanol flame the measured values of allyl radical are closer to model predictions.

Propylene: This species is over-predicted for both fuels. Comparisons with the experimental data of Kasper et al. [32] do not confirm this deviation.

1-Butene and butadiene: These species are under-predicted by a factor 2 in *n*-propanol flame, while a closer agreement is observed in *iso*-propanol flame.

Diacetylene and vinylacetylene: These species are largely under-predicted in all the flames and C_4H_5 radical shows the same deviation.

Benzene: The predicted peak value of this species is \sim one half of the measured value in *n*-propanol flame, while the predictions are double of the measured value in the *iso*-propanol flame. The predicted values are consistent with those measured by Kasper et al. [32] employing the PI technique, but both are under-predicted when compared with those measured employing the EI technique.

Pentadiene and cyclopentadiene: Predicted values of these species show satisfactory agreement with experimental data.

The availability of this double set of very accurate experimental data is of course of extreme value for the kinetic modeling activity. In addition, model results could be of potential interest

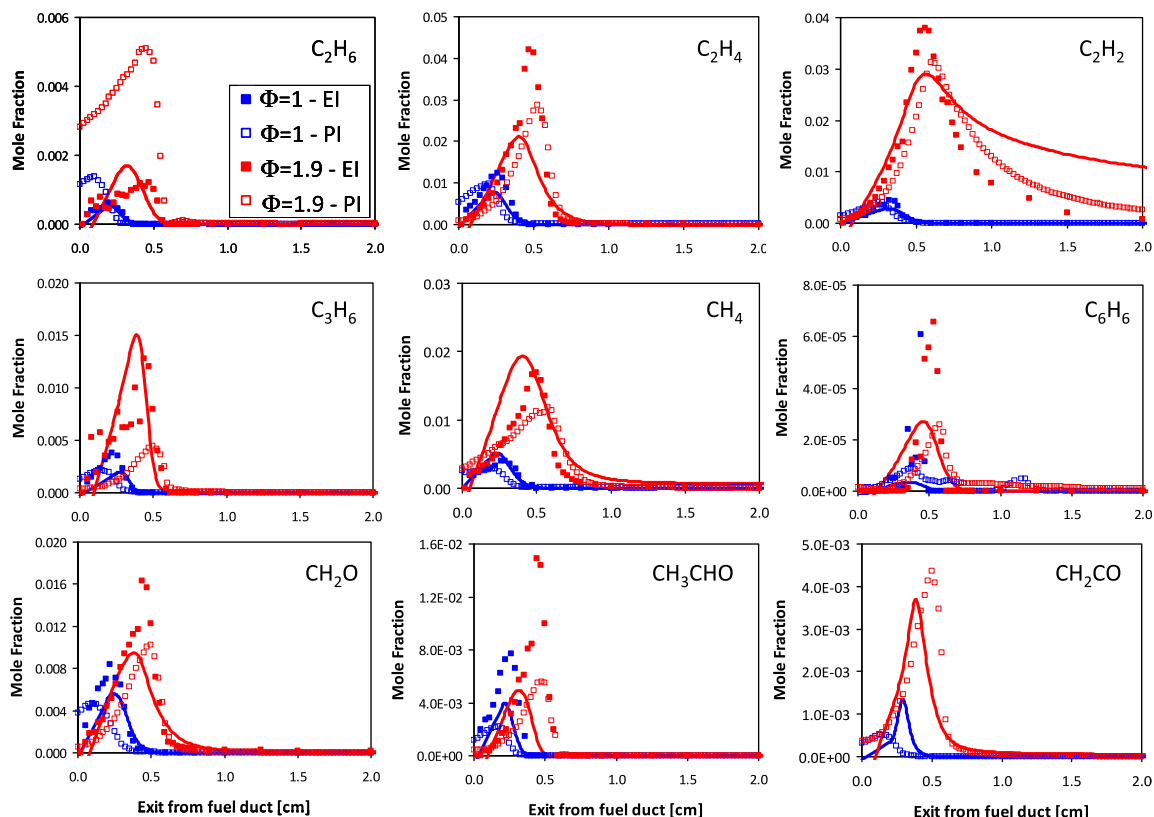


Fig. 12. Profiles of mole fraction of various intermediate species as a function of distance from the fuel duct. The fuel tested is *n*-propanol. The equivalence ratio is $\Phi = 1$, and $\Phi = 1.9$. The symbols represent experimental data measured by Kasper et al. [32] using electron ionization (EI) and photon ionization (PI) molecular-beam mass spectrometry. The curves are model predictions.

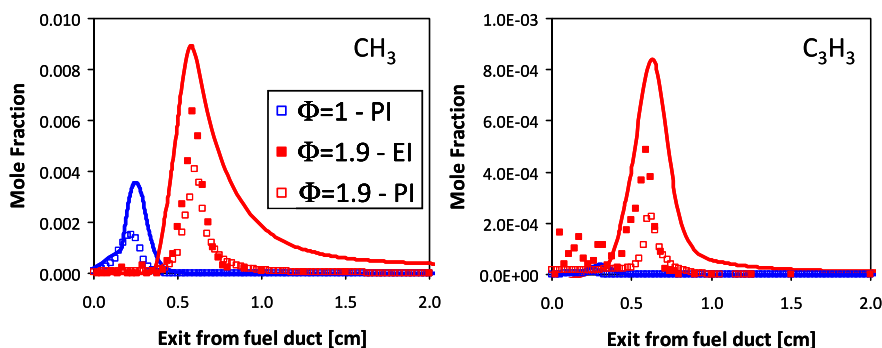


Fig. 13. Profiles of mole fraction of methyl (CH_3) radical and propargyl (C_3H_3) radical as a function of distance from the fuel duct. The fuel tested is *iso*-propanol. The equivalence ratio is $\Phi = 1$, and $\Phi = 1.9$. The symbols represent experimental data measured by Kasper et al. [32] using electron ionization (EI) and photon ionization (PI) molecular-beam mass spectrometry. The curves are model predictions.

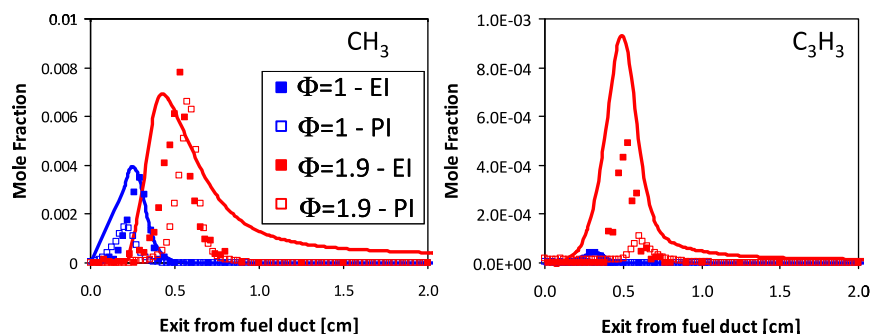


Fig. 14. Profiles of mole fraction of methyl (CH_3) radical and propargyl (C_3H_3) radical as a function of distance from the fuel duct. The fuel tested is *n*-propanol. The equivalence ratio is $\Phi = 1$, and $\Phi = 1.9$. The symbols represent experimental data measured by Kasper et al. [32] using electron ionization (EI) and photon ionization (PI) molecular-beam mass spectrometry. The curves are model predictions.

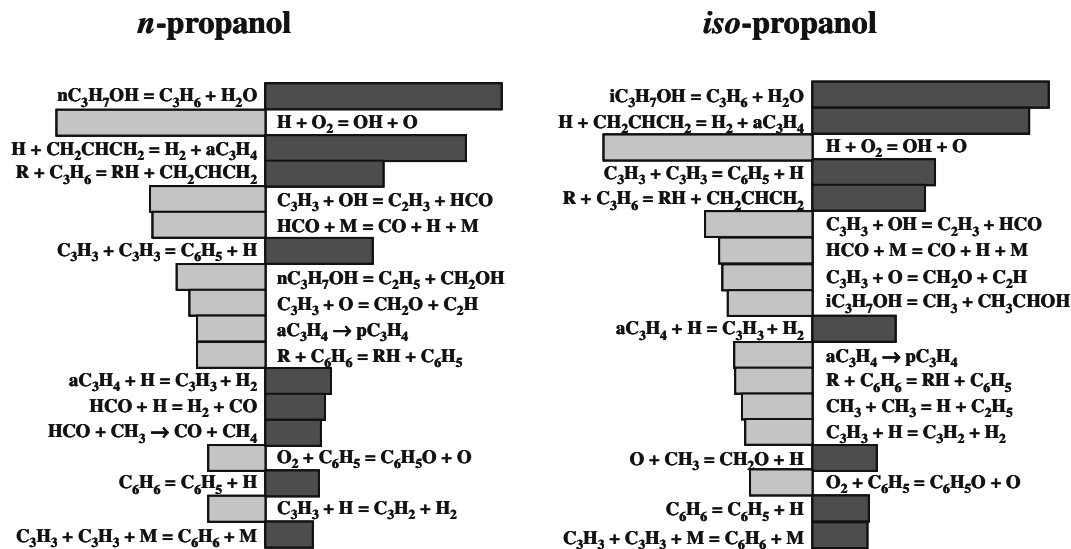


Fig. 15. Sensitivity coefficients for benzene formation in *n*-propanol and *iso*-propanol flames [32] a $\phi = 1.9$. Sensitivity coefficients refer to the axial location corresponding to the benzene maxima in the flames. Dark bars correspond to positive sensitivity coefficients.

to further improve the experimental accuracy and/or experimental methods.

6. Summary and conclusions

A kinetic mechanism that describes the primary reactions of combustion of *n*-propanol and *iso*-propanol is developed. This primary mechanism is appended to a previously developed detailed scheme of pyrolysis and oxidation of hydrocarbon fuels. The main effect arising from the presence of hydroxyl group in alcohols was on the α position in the H-abstraction reactions and radical decom-

positions. Employing a systematic approach for the metathesis reactions and some lumping procedure for fast intermediate radicals, a small subset of new primary reactions were developed for describing combustion of *n*-propanol and *iso*-propanol. Four-center molecular dehydration reaction to form propylene is mainly relevant for *iso*-propanol. New experimental data on counterflow non-premixed flames were obtained for mechanism validation. Flame structures were measured under similar conditions for both fuels to elucidate the similarities and differences in combustion characteristics of the two isomers. The profiles measured include those of formaldehyde, acetaldehyde, propanal, and acetone. The

Table 2
Comparison of predicted peak position and maximum mole fractions (X_{\max}) of the rich flames of *n*-propanol and *iso*-propanol with experimental data. The experimental data are those of Li et al. [31].

Formula	Species	Rich <i>n</i> -propanol flame				Rich <i>iso</i> -propanol flame			
		Position (cm)		X_{\max}		Position (cm)		X_{\max}	
		Pred. ^a	Exp	Pred.	Exp	Pred. ^b	Exp	Pred.	Exp
CH ₃	Methyl radical	0.76	0.85	6.1×10^{-03}	6.8×10^{-03}	0.84	0.85	8.1×10^{-03}	4.9×10^{-03}
C ₂ H ₂	Acetylene	0.87	0.85	1.9×10^{-02}	1.8×10^{-02}	0.98	0.9	1.9×10^{-02}	5.6×10^{-03}
C ₂ H ₃	Vinyl radical	0.78	0.85	1.6×10^{-04}	3.0×10^{-05}	0.91	0.95	1.1×10^{-04}	1.1×10^{-05}
C ₂ H ₄	Ethylene	0.72	0.75	1.4×10^{-02}	1.9×10^{-02}	0.84	0.8	1.0×10^{-02}	5.7×10^{-03}
HCO	Formyl radical	0.8	0.7	3.2×10^{-04}	4.1×10^{-05}	0.91	0.85	2.5×10^{-04}	2.0×10^{-05}
H ₂ CO	Formaldehyde	0.69	0.7	6.7×10^{-03}	6.9×10^{-03}	0.82	0.65	5.0×10^{-03}	2.8×10^{-03}
CH ₃ OH	Methanol	0.59	0.5	1.1×10^{-03}	8.1×10^{-04}	0.57	0.5	6.2×10^{-04}	2.9×10^{-04}
C ₃ H ₃	Propargyl radical	0.81	0.85	5.1×10^{-04}	3.3×10^{-04}	0.91	0.95	7.3×10^{-04}	3.4×10^{-04}
C ₃ H ₄	Propyne	0.82	0.8	4.1×10^{-04}	5.6×10^{-04}	0.89	0.85	6.5×10^{-04}	4.6×10^{-04}
C ₃ H ₄	Allene	0.77	0.75	3.6×10^{-04}	2.5×10^{-04}	0.85	0.85	6.0×10^{-04}	1.8×10^{-04}
C ₃ H ₅	Allyl radical	0.82	0.8	1.4×10^{-03}	1.4×10^{-04}	0.89	0.9	1.8×10^{-03}	1.4×10^{-04}
C ₂ H ₂ O	Ketene	0.72	0.7	2.4×10^{-03}	1.2×10^{-03}	0.77	0.8	3.8×10^{-03}	3.9×10^{-03}
C ₃ H ₆	Propylene	0.72	0.7	7.5×10^{-03}	2.5×10^{-03}	0.77	0.8	1.4×10^{-02}	3.9×10^{-03}
C ₂ H ₄ O	Acetaldehyde	0.63	0.65	4.5×10^{-03}	5.2×10^{-03}	0.74	0.65	3.8×10^{-03}	1.1×10^{-03}
C ₄ H ₂	Diacetylene	0.92	0.95	8.0×10^{-05}	4.7×10^{-04}	1	1	9.8×10^{-05}	2.4×10^{-04}
C ₄ H ₄	Vinylacetylene	0.77	0.85	1.8×10^{-05}	1.3×10^{-04}	0.87	0.9	3.9×10^{-05}	1.6×10^{-04}
C ₄ H ₅	But-2-yn-1-yl radical	0.63	0.7	4.2×10^{-07}	4.9×10^{-06}	0.6	0.95	3.3×10^{-07}	9.9×10^{-06}
C ₄ H ₆	1,3-Butadiene	0.72	0.75	4.3×10^{-05}	9.1×10^{-05}	0.79	0.85	1.2×10^{-04}	1.4×10^{-04}
C ₄ H ₈	1-Butene	0.67	0.7	6.2×10^{-05}	1.2×10^{-04}	0.72	0.75	2.2×10^{-04}	1.7×10^{-04}
C ₃ H ₆ O	Propanal	0.64	0.55	2.9×10^{-03}	2.2×10^{-03}	0.64	nd	1.0×10^{-05}	nd
C ₃ H ₆ O	Acetone	0.97	nd	2.2×10^{-05}	nd	0.67	0.75	6.5×10^{-03}	5.3×10^{-03}
C ₅ H ₆	1,3-Cyclopentadiene	0.74	0.8	1.1×10^{-05}	1.5×10^{-05}	0.82	0.85	3.3×10^{-05}	2.8×10^{-05}
C ₅ H ₈	1,3-Pentadiene	0.76	0.7	4.6×10^{-06}	6.0×10^{-06}	0.84	0.75	8.5×10^{-06}	9.4×10^{-06}
C ₆ H ₆	Benzene	0.74	0.7	7.6×10^{-06}	1.4×10^{-05}	0.86	0.85	2.3×10^{-05}	1.3×10^{-05}

^a Predicted values are shifted of 0.52 cm.

^b Predicted values are shifted of 0.44 cm.

validation of the kinetic model was extended to different sets of experimental data obtained by other investigators in very different operative conditions and reaction configurations. The agreement between the kinetic model and experimental data was generally satisfactory, in terms of reactivity and selectivity in major products and minor species. The flame structures and overall combustion characteristics of *n*-propanol and *iso*-propanol are found to be similar. Modeling shows that ethylene is only a secondary product of *iso*-propanol combustion and its amount is significantly lower. Acetone is formed under all conditions in *iso*-propanol flames, while propanal is formed in *n*-propanol flames. The kinetic model developed here is expected to be the starting point for extension to higher alcohols.

Acknowledgments

The authors acknowledge the valuable discussions with Professor M. Dente and the useful work of R. Grana. The Authors further acknowledge Professor M. J. Thompson, T. Kasper and H. Curran for providing detailed information and further insight on their experimental data. The authors appreciate the use of the shock tube experimental data of Fig. 6 by Johnson et al. prior to their publication. The research at the University of California at San Diego is supported by UC Discovery/Westbiofuels, Grant # GCP06-10228. The research activity of Politecnico was supported by the European Community in the behalf of the DREAM Project (FP7-211861) and by CNR-DET (MAP/MSE Biofuel Program).

Appendix A. Supplementary material

Supplementary data associated with this article can be found, in the online version, at doi:10.1016/j.combustflame.2009.09.002.

References

- [1] S.R. Smith, A.S. Gordon, Studies of diffusion flames. II. Diffusion flames of some simple alcohols, *Journal of Physical Chemistry* 60 (8) (1956) 1059–1062.
- [2] K. Seshadri, Structure and extinction of laminar diffusion flames above condensed fuels with water and nitrogen, *Combustion and Flame* 33 (1978) 197–215.
- [3] A. Hamins, K. Seshadri, The influence of alcohols on the combustion of hydrocarbon fuels in diffusion flames, *Combustion and Flame* 64 (1986) 43–54.
- [4] A. Hamins, K. Seshadri, The structure of diffusion flames burning pure, binary, and ternary solutions of methanol, heptane, and toluene, *Combustion and Flame* 68 (1987) 295–307.
- [5] S.C. Li, F.A. Williams, Experimental and numerical studies of two-stage methanol flames, in: *Proceedings of the Combustion Institute*, vol. 26, 1996, pp. 1017–1024.
- [6] T. Held, F. Dryer, A comprehensive mechanism for methanol oxidation, *International Journal of Chemical Kinetics* 118 (1998) 805–830.
- [7] O.L. Gülder, Laminar burning velocities of methanol, ethanol and isooctane–air mixtures, in: *Proceedings of the Combustion Institute*, 1982, pp. 275–281.
- [8] N. Marinov, A detailed kinetic model for high temperature ethanol oxidation, *International Journal of Chemical Kinetics* 31 (1999) 183–220.
- [9] R. Seiser, S. Humer, K. Seshadri, E. Pucher, Experimental investigation of methanol and ethanol flames in nonuniform flows, in: *Proceedings of the Combustion Institute*, vol. 31, 2007, pp. 1173–1180.
- [10] T.S. Norton, F.L. Dryer, The flow reactor oxidation of C1–C4 alcohols and MTBE, in: *Proceedings of the Combustion Institute*, vol. 23, 1990, pp. 179–185.
- [11] F. N. Egolopoulos, D. X. Lu, and C. K. Law, A study on ethanol oxidation kinetics in laminar premixed flames, flow reactors and shock tubes, in: *Proceedings of the Combustion Institute*, vol. 24, 1992, pp. 833–841.
- [12] W. Tsang, Energy transfer effects during the multichannel decomposition of ethanol, *International Journal of Chemical Kinetics* 36 (8) (2004) 456–465.
- [13] P. Saxena, F.A. Williams, Numerical and experimental studies of ethanol flames, in: *Proceedings of the Combustion Institute*, vol. 31, 2007, pp. 1149–1156.
- [14] P. Dagaut, C. Togbé, Experimental and modeling study of the kinetics of oxidation of ethanol–gasoline surrogate mixtures (E85 surrogate) in a jet-stirred reactor, *Energy & Fuels* 22 (2008) 3499–3505.
- [15] M. Abián, C. Esarte, A. Millera, R. Bilbao, M.U. Alzueta, Oxidation of acetylene–ethanol mixtures and their interaction with NO, *Energy & Fuels* 22 (2008) 3814–3823.
- [16] A. Frassoldati, A. Cuoci, T. Faravelli, E. Ranzi, Kinetic modeling of the oxidation of ethanol and gasoline surrogate mixtures, *Combustion Science and Technology*, 2009, in press.
- [17] C. McEnally, L. D. Pfefferle, Fuel decomposition and hydrocarbon growth processes for oxygenated hydrocarbons: butyl alcohols, in: *Proceedings of the Combustion Institute*, vol. 30, 2005, pp. 1363–1370.
- [18] B. Yang, P. Oßwald, Y. Li, J. Wang, L. Wei, Z. Tian, F. Qi, K. Kohse-Höinghaus, Identification of combustion intermediates in isomeric fuel-rich premixed butanol–oxygen flames at low pressure, *Combustion and Flame* 148 (2007) 198–209.
- [19] P. Dagaut, C. Togbé, Oxidation kinetics of butanol–gasoline surrogate mixture in a jet-stirred reactor: experimental and modeling study, *Fuel* 87 (2008) 3313–3321.
- [20] J.T. Moss, A.M. Berkowitz, M.A. Oehlschlaeger, J. Biet, A. Warth, P.A. Glaude, F. Battin-Leclerc, An experimental and kinetic modelling study of the oxidation of four isomers of butanol, *Journal of Physical Chemistry* 112 (2008) 1084–10855.
- [21] J. Moc, J.M. Simmie, H.J. Curran, The elimination of water from a conformationally complex alcohol: a computational study of the gas phase dehydration of *n*-butanol, *Journal of Molecular Structure* 928 (2009) 149–157.
- [22] S.M. Sarathy, M.J. Thomson, C. Togbé, P. Dagaut, F. Halter, C. Mountaim-Rousselle, An experimental and kinetic modeling study of *n*-butanol combustion, *Combustion and Flame* 156 (2009) 852–864.
- [23] R. Wang, P. Cadman, Soot and pah production from spray combustion of different hydrocarbons behind reflected shock waves, *Combustion and Flame* 112 (1998) 359–370.
- [24] J.A. Barnard, H.W.D. Hughes, The pyrolysis of *n*-propanol, *Transactions of the Faraday Society* 56 (1) (1960) 64–71.
- [25] J.A. Barnard, The pyrolysis of *iso*-propanol, *Transactions of the Faraday Society* 56 (1) (1960) 72–79.
- [26] A.B. Trenwith, Thermal decomposition of isopropanol, *Journal of the Chemical Society, Faraday Transactions 1: Physical Chemistry in Condensed Phases* 71 (1975) 2405–2412.
- [27] B.H. Bui, R.S. Zhu, M.C. Lin, Thermal decomposition of *iso*-propanol: first-principles prediction of total and product-branching rate constants, *Journal of Chemical Physics* 117 (24) (2002) 11188–11195.
- [28] J. Cai, F. Li, W.A. Sirignano, Three-dimensional structures of flames over liquid fuel pools, *Combustion Science and Technology* 175 (2003) 2113–2139.
- [29] A. Sinha, M.J. Thomson, The chemical structures of opposed flow diffusion flames of C3 oxygenated hydrocarbons (*iso*-propanol, dimethoxymethane, and dimethyl carbonate) and their mixtures, *Combustion and Flame* 136 (2004) 548–556.
- [30] B.D. Shaw, J.B. Wei, Propanol droplet flammability and combustion in air-diluent environments under normal and reduced gravity, *Combustion Science and Technology* 179 (2007) 1205–1223.
- [31] Y. Li, L. Wei, Z. Tian, B. Yang, J. Wang, T. Zhang, F. Qi, A comprehensive experimental study of low-pressure premixed C3-oxygenated hydrocarbon flames with tunable synchrotron photoionization, *Combustion and Flame* 152 (2008) 336–359.
- [32] T. Kasper, P. Oßwald, U. Struckmeier, K. Kohse-Höinghaus, C.A. Taatjes, J. Wang, T.A. Cool, M.E. Law, A. Morel, P.R. Westmoreland, Combustion chemistry of propanol isomers—investigated by electron ionization and VUV-photoionization molecular-beam mass spectrometry, *Combustion and Flame* 156 (2009) 1181–1201.
- [33] M.V. Johnson, S.S. Goldsborough, E. Larkin, G. OMalley, Z. Serinyel, P. OToole, H.J. Curran, Ignition delay measurements of *n*-propanol and *iso*-propanol in a shock tube, in: *Proceedings of the 6th US National Combustion Meeting, Paper # 22C5*, The University of Michigan, Ann Arbor, Michigan, USA, May 17–20, 2009, The Combustion Institute, 2009.
- [34] M.Z. Jacobson, Effects of ethanol (E85) versus gasoline vehicles on cancer and mortality in the United States, *Environmental Science and Technology* 41 (11) (2007) 4150–4157.
- [35] E. Zervas, X. Montagne, J. Lahaye, Emission of alcohols and carbonyl compounds from spark ignition engine influence of fuel and air/fuel equivalence ratio, *Environmental Science and Technology* 36 (2002) 2414–2421.
- [36] F.A. Williams, *Combustion Theory*, second ed., Addison-Wesley Publishing Company, Redwood City, CA, 1985.
- [37] A. Liñán, F.A. Williams, *Fundamental Aspects of Combustion*, volume 34 of Oxford Engineering Science Series, Oxford University Press, New York, 1993.
- [38] N. Peters, Local quenching due to flame stretch and non-premixed turbulent combustion, *Combustion Science and Technology* 30 (1983).
- [39] N. Peters, *Turbulent Combustion*, Cambridge University Press, Cambridge, England, 2000.
- [40] K. Seshadri, F.A. Williams, Laminar flow between parallel plates with injection of a reactant at high Reynolds number, *International Journal of Heat and Mass Transfer* 21 (2) (1978) 251–253.
- [41] A. Galano, J.R. Alvarez-Idaboy, G. Bravo-Perez, M.E. Ruiz-Santoyo, Gas phase reactions of C1–C4 alcohols with the OH radical: a quantum mechanical approach, *Physical Chemistry Chemical Physics Journal* 4 (2002) 4648–4662.
- [42] R. Atkinson, D.L. Baulch, R.A. Cox, R.F. Hampson Jr., J.A. Kerr, M.J. Rossi, J. Troe, Evaluated kinetic, photochemical and heterogeneous data for atmospheric chemistry: supplement V. IUPAC subcommittee on gas kinetic data evaluation for atmospheric chemistry, *Journal of Physical and Chemical Reference Data* 26 (1997) 521–1011.

- [43] R. Atkinson, D.L. Baulch, R.A. Cox, R.F. Hampson Jr., J.A. Kerr, M.J. Rossi, J. Troe, Evaluated kinetic and photochemical data for atmospheric chemistry, organic species: supplement VII, *Journal of Physical and Chemical Reference Data* 28 (1999) 191–394.
- [44] J.R. Dunlop, F.P. Tully, Catalytic dehydration of alcohols by hydroxyl: 2-propanol; an intermediate case, *Journal of Physical Chemistry B* 97 (1993) 6457–6464.
- [45] E. Ranzi, M. Dente, T. Faravelli, G. Pennati, Prediction of kinetic parameters for hydrogen abstraction reactions, *Combustion Science and Technology* 95 (1983) 1–50.
- [46] E. Ranzi, T. Faravelli, P. Gaffuri, G.C. Pennati, A. Sogaro, A wide range modeling study of propane and *n*-butane oxidation, *Combustion Science and Technology* 100 (1994) 299–330.
- [47] E. Ranzi, M. Dente, A. Goldaniga, G. Bozzano, T. Faravelli, Lumping procedures in detailed kinetic modeling of gasification, pyrolysis, partial oxidation and combustion of hydrocarbon mixtures, *Progress in Energy and Combustion Science* 27 (2001) 99–139.
- [48] H.J. Curran, Rate constant estimation for C1 to C4 alkyl and alkoxy radical decomposition, *International Journal of Chemical Kinetics* 38 (4) (2006) 250–275.
- [49] C.G. Newman, H.E. O'Neal, M.A. Ring, F. Leska, N. Shipley, Kinetics and mechanism of the silane decomposition, *International Journal of Chemical Kinetics* 11 (1979) 1167–1182.
- [50] E. Ranzi, T. Faravelli, A. Frassoldati, S. Granata, Wide range kinetic modeling study of pyrolysis and combustion of heavy *n*-alkanes, *Industrial and Engineering Chemistry Research* 44 (14) (2005) 5170–5183.
- [51] R.J. Kee, F. Rupley, J.A. Miller, The Chemkin thermodynamic data base, Report sand86-8215b, Sandia National Laboratories, Livermore, California, 1987.
- [52] R.J. Kee, F. Rupley, J.A. Miller, The Chemkin thermodynamic data base, Technical report, Sandia National Laboratories, Livermore, California, 1989.
- [53] S.W. Benson, *Thermochemical Kinetics*, second ed., Wiley, New York, 1996.
- [54] <<http://www.chem.polimi.it/CRECKModeling>>.
- [55] D. Manca, G. Buzzi-Ferraris, T. Faravelli, E. Ranzi, Numerical problems in the solution of oxidation and combustion models, *Combustion Theory and Modelling* 5 (2) (2001) 185–199.
- [56] A. Cuoci, A. Frassoldati, T. Faravelli, E. Ranzi, Frequency response of counter flow diffusion flames to strain rate harmonic oscillations, *Combustion Science and Technology* 180 (2008) 767–784.
- [57] G. Buzzi-Ferraris, *Building Numerical Libraries the Object-Oriented Way*, Addison Wesley/Longman, 1993.
- [58] G. Buzzi-Ferraris, Numerical libraries in c++. Politecnico di Milano – Freely available at the web address: <<http://www.chem.polimi.it/homes/gbuzzi>>.
- [59] T. Kasper, Personal communication, 2009.